

# Multiple Angles of Arrival Estimation Using Broadband Signals and a Nonuniform Planar Array

Chao Liu, *Member, IEEE*, Bensheng Yang, *Member, IEEE*, Peize Zhang, *Member, IEEE*,  
Haiming Wang, *Member, IEEE*, Cheng-Xiang Wang, *Fellow, IEEE*, and Xiaohu You, *Fellow, IEEE*

**Abstract**—As the requirements related to resolution or the data rate increase, most angle-of-arrival (AoA) estimation problems can be assumed to be under a broadband signal model. In this paper, AoA estimation using a nonuniform planar array (NUPA), which aims to resolve more signals and reduce mutual coupling, is considered under a broadband signal model. The analysis is conducted in both the space and frequency domains, and a broadband co-array is proposed to improve the performance of the AoA estimation. The broadband co-array is generated as follows: First, the received broadband signal is decomposed into several narrowband signals, and the samples from different frequency bins are transformed to space-domain samples to generate a virtual array. Then, the second-order statistics of the virtual array are used to generate the broadband co-array. The virtual array can decrease the number of element pairs with small interelement spacing to reduce mutual coupling in AoA estimations. With the help of the virtual array, the following broadband co-array can greatly increase the degrees of freedom, resulting in more resolvable signals and lower Cramer-Rao bounds of AoA estimation. An optimization method based on sparse recovery is proposed to locate the array. The simulation results confirm the AoA estimation performance achieved by the designed NUPA.

**Index Terms**—Nonuniform planar array (NUPA), broadband signals, visualization, optimization of array pattern, co-array, AoA estimation.

## I. INTRODUCTION

Accurate angle-of-arrival (AoA) estimations play important roles in many applications, such as radar, astronomy

Manuscript received March 25, 2021; revised Apr. 7, 2022; accepted Apr. 16, 2022. Date of publication ; date of current . This work was supported in part by the National Key R&D Program of China under Grant 2020YFB1804901, the National Natural Science Foundation of China under Grant 61960206006, and the Keysight's University Research Collaborations program.

H. M. Wang is with the State Key Laboratory of Millimeter Waves, Southeast University, Nanjing 210096, China and the Pervasive Communication Research Center, Purple Mountain Laboratories, Nanjing 211111, China (e-mail: hmwang@seu.edu.cn). (Corresponding author: Haiming Wang.)

C. Liu is with the Pervasive Communication Research Center, Purple Mountain Laboratories, Nanjing 211111, China (e-mail: liuchao@pmlabs.com.cn).

B. S. Yang was with the State Key Laboratory of Millimeter Waves, Southeast University, Nanjing 210096, China and is currently with Huawei Software Technologies Co., Ltd., Nanjing 210012, China (e-mail: yangbensheng2@huawei.com).

P. Z. Zhang is with the State Key Laboratory of Millimeter Waves, Southeast University, Nanjing 210096, China. (e-mail: pzzhang@seu.edu.cn).

C. X. Wang and X. H. You are with the National Mobile Communications Research Laboratory, Southeast University, Nanjing 210096, China, and the Pervasive Communication Research Center, Purple Mountain Laboratories, Nanjing 211111, China (e-mail: chxwang@seu.edu.cn; xhyu@seu.edu.cn).

Color versions of one or more of the figures in this paper are available online at <http://ieeexplore.ieee.org>.

Digital Object Identifier

and communications [1]–[6]. Classic AoA estimation methods, i.e., multiple signal classification (MUSIC) [7], estimation of signal parameters via rotational invariance techniques (ES-PRIT) [8], and their generalizations [9], [10], have been widely studied. To achieve high precision, various estimation methods [11], [12] have been developed to approach the Cramer-Rao bound (CRB) [13], which expresses the minimum achievable variance on AoAs. An extended direction of arrival (DoA)-matrix method, which can make full use of the information in the autocorrelation and cross-correlation matrices, was studied to enhance the performance [11]. A high-resolution AoA method was proposed under the hybrid analog and digital structure [12]. In fact, it can also be inferred from the CRB that the location of an array impacts the estimation performance. Furthermore, most methods are confined to the case of traditional arrays, i.e., uniform linear arrays (ULAs), which suffer from significant mutual coupling brought by many element pairs with small interelement spacing (IES) [14]–[16] and limit the number of resolvable signals.

Nonuniform arrays, which are used to resolve more signals and reduce mutual coupling effects, have been widely investigated. Previous works on nonuniform arrays include [17]–[29]. The number of sensor pairs with small IESs in nonuniform arrays is usually much smaller than that in ULAs, so nonuniform arrays lead to lower mutual coupling. Furthermore, with the help of co-arrays [20], nonuniform arrays can dramatically increase the degrees of freedom (DoFs). Using only the second-order statistics of the impinging signals, an array with  $M$  physical elements can generate a co-array yielding  $O(M^2)$  DoFs [20]. Classic one-dimensional (1-D) nonuniform arrays include the minimum redundancy array [19], nested array [20], the coprime array [18], super nested array [21] and other generalizations. A co-array is generated from the second-order statistics, and the AoA is estimated via spectral or sparsity-based methods [30]–[32]. The designed arrays should have co-arrays that are hole-free or offer high DoFs. Experiments have also been conducted to confirm the effectiveness of nonuniform arrays [22].

To sense high-dimensional space, two-dimensional (2D) nonuniform arrays, i.e., billboard arrays [29], open box arrays [28], 2D coprime arrays [23], [26], hourglass arrays [24] and 2D nested arrays [25], [27] were studied. A 2D coprime array is derived by extending a 1-D coprime array to a 2D nonuniform array. The coprime planar array geometry, which consists of two uniform planar subarrays the size of two coprime integers, was proposed in [26], and a new 2D coprime array was further proposed to increase the DoFs and

enhance the estimation performance [23]. Hourglass arrays were proposed to reduce the mutual coupling in open box arrays [24]. A 2D nested array was obtained by systematically nesting two arrays, one with sensors on a sparse lattice and the other on a dense lattice, where the lattices have a certain relation with each other [25], [27].

Using the studied nonuniform arrays, the corresponding AoA estimation methods were proposed [33]–[36]. The 2D AoA estimation method using parallel coprime arrays and parallel nested arrays were developed in [33] and [35], respectively. In [35], AoA estimation for coprime multiple-input multiple-output radar was studied, and a combined unitary estimation of signal parameters via an ESPRIT-based algorithm was proposed. A novel virtual array interpolation-based method for coprime arrays was proposed to enhance the AoA estimation performance [36].

A narrowband signal is assumed for 2D nonuniform arrays in [23]–[27], [29] and the corresponding AoA estimation methods in [33]–[36]. As the requirements related to resolution or the data rate increase, the signal bandwidth increasingly widens [37]. Using broadband signals, coherent signal subspace methods (CSSMs), which design focusing matrices to combine the information from different frequency subbands, have been studied [38]–[40]. However, CSSM requires the input of initial values to find focusing matrices, and poor initial values can lead to biased estimates [41]. The existence of the beamforming matrix depends on the size of the field of view, and the performance of focusing matrices dramatically decreases when the bandwidth becomes too wide. Using these methods, the number of resolvable signals is still limited by the number of physical elements. In [42], the method of wideband direction of arrival (DoA) estimation with sparse linear arrays, which uses Jacobi-Anger expansion to express the received signal, was studied, and its superior performance was shown. However, Jacobi-Anger expansion cannot be directly extended to 2D arrays.

In this study, on the basis of broadband signals, an NUPA is proposed to estimate multiple AoAs. The element locations in the proposed NUPA are then obtained by exploiting the benefit of broadband signals and optimizing the performance of the broadband co-array. The broadband co-array is obtained in two steps. In the first step, the relationship between frequency-domain samples and space-domain samples is studied to generate a virtual array. In the second step, the second-order statistics of the virtual array are used to generate a broadband co-array. The contributions of this paper are summarized as follows:

- First, the relationship between frequency- and space-domain samples is exploited. Under certain conditions related to the array aperture and relative bandwidth of the transmitted signal, frequency-domain samples can be transformed into space-domain samples to generate a virtual array. The maximum number of virtual elements is also analyzed, and the proposed broadband co-array can enhance the benefits achieved by the virtual array to resolve more signals and lower the CRB of the AoA.
- Second, a physical element and a virtual element or two virtual elements contributed by the virtual array can be

used to format an element pair with a small IES to perform Nyquist sampling in the space domain. Thus, the number of physical element pairs with small IESs is largely decreased to reduce mutual coupling.

- Third, the concept of broadband co-arrays is extended to existing arrays to enhance the AoA estimation performance. To ensure the estimation performance in scenarios with fewer elements, a method that optimizes the broadband co-array performance is proposed for locating elements.

The rest of this paper is organized as follows. In Section II, the signal model is presented. In Section III, AoA estimation of broadband signals using NUPA is considered. In Section IV, CRB analysis is performed. Simulations are conducted to confirm the effectiveness of the proposed NUPA in Section V. Finally, Section VI concludes this paper.

*Notations:* We use upper (lower) bold-face letters to denote matrices (vectors). Superscript  $(\cdot)^H$  denotes the Hermitian transpose,  $(\cdot)^T$  denotes the transpose, and  $(\cdot)^*$  denotes the complex conjugate.  $\otimes$  represents the Kronecker product, and  $\odot$  represents the Khatri-Rao product (i.e., the columnwise Kronecker product). We use  $\text{vec}\{\cdot\}$  to denote matrix vectorization and  $\lfloor \cdot \rfloor$  to denote the floor operation.

## II. SYSTEM MODEL

Suppose  $K$  broadband uncorrelated signals with bandwidth  $B$  impinge on a planar array with  $M$  elements. The  $m$ -th element is assumed to be placed on the grid  $(i_m d, j_m d)$  ( $1 \leq m \leq M$ ), where  $(i_m, j_m)$  is a nonnegative integer-valued vector and  $d$  is the half-wavelength corresponding to carrier frequency  $f_c$ . The elements are assumed to be located at  $\mathbb{M} = \{(d i_m, d j_m)\}$ . A diagram of the signal model for a physical array is displayed in Fig. 1(a). At each element, the received broadband signal is first sampled at the Nyquist rate, and the samples are then partitioned into  $Q$  frequency subbands by discrete Fourier transform. Assume that the frequency of broadband signals is divided into  $Q$  subbands and that the discrete frequency axis is set as  $[f_1, f_2, \dots, f_Q]$ , where  $f_q = f_c - B/2 + (q - 1)B/(Q - 1)$ . For the received broadband signal, the  $n$ -th snapshot of array  $\mathbb{M}$  at frequency  $f_q$  is denoted as

$$\mathbf{r}_{\mathbb{M},q,n} = \mathbf{C} \sum_{k=1}^K \rho_{k,n} \mathbf{a}_{\mathbb{M},k,q} + \mathbf{n}_{\mathbb{M},q,n}, \quad (1)$$

where  $\mathbf{C}$  is the mutual coupling matrix [14] and  $\rho_{k,n}$  is the amplitude of the  $k$ -th signal ( $1 \leq k \leq K$ ) at the  $n$ -th snapshot. The transmitted signal is assumed to have a flat spectrum, i.e., phase-modulated orthogonal frequency division multiplexing (OFDM) signal, and is known to the receiver. In (1), the frequency envelope of the transmitted signal has been removed from the received broadband signal  $\mathbf{r}_{\mathbb{M},q,n}$  in the pre-processing stage. Therefore, the amplitude  $\rho_{k,n}$  is assumed to be uncorrelated with frequency and the transmitted signal.  $\mathbf{n}_{\mathbb{M},q,n}$  denotes the noise at frequency  $f_q$ , and  $\mathbf{a}_{\mathbb{M},k,q}$  is the steering vector of the  $k$ -th signal at frequency  $f_q$ , which is denoted as follows:

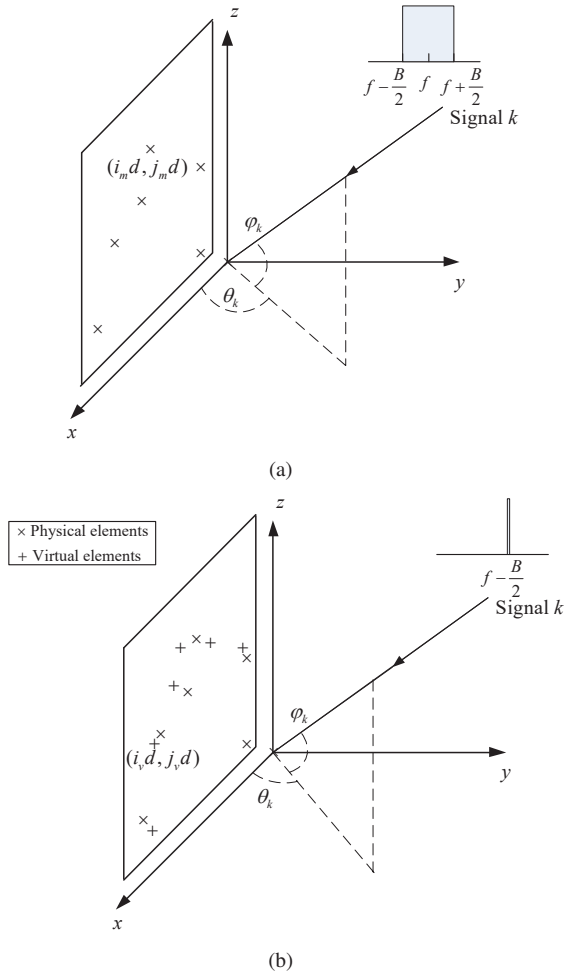


Fig. 1. Diagram of the signal model: (a) Physical array; (b) Virtual array.

$$\mathbf{a}_{\mathbb{M},k,q} = [a_{1,k,q}, a_{2,k,q}, \dots, a_{M,k,q}]^T, \quad (2)$$

where

$$a_{m,k,q} = e^{-j2\pi \frac{(\mathbf{u}_m)^T \mathbf{b}_k}{c} f_q}, \quad (3)$$

$$\mathbf{u}_m = [i_m d, j_m d]^T, \quad (4)$$

$$\mathbf{b}_k = [\cos \varphi_k \cos \theta_k, \sin \varphi_k]^T, \quad (5)$$

with  $(\varphi_k, \theta_k)$  denoting the AoA of the  $k$ -th signal and  $c$  denoting the speed of the wave.

The signals are assumed to follow the unconditional model [43] and to be temporally uncorrelated  $\mathbb{E}\{\rho_{k,n}(\rho_{k',n'})^*\} = 0$ . The power of the  $k$ -th signal is  $\sigma_k^2$ . The noise  $\mathbf{n}_{\mathbb{M},q,n}$  is additive white Gaussian noise with variance  $\sigma_0^2$ .

In this study, we do not consider the gain and phase calibration and AoA estimation simultaneously and assume that the gain and phase impairments of NUPA have been calibrated. Though gain and phase impairments for NUPA could be more challenging to be dealt with than those for simple uniform linear arrays, some recent studies [44], [45] can be directly used to estimate gain and phase impairments beforehand.

When mutual coupling is absent, the received signal can be simplified from (1) as follows:

$$\mathbf{r}_{\mathbb{M},q,n} = \sum_{k=1}^K \rho_{k,n} \mathbf{a}_{\mathbb{M},k,q} + \mathbf{n}_{\mathbb{M},q,n}. \quad (6)$$

Under the assumption of the narrowband signal model, the spatial samples are acquired at carrier frequency  $f_c$  and can be derived from (6) as follows:

$$\mathbf{r}_{\mathbb{M},n} = \sum_{k=1}^K \rho_{k,n} \mathbf{a}_{\mathbb{M},k} + \mathbf{n}_{\mathbb{M},n}, \quad (7)$$

where

$$\mathbf{a}_{\mathbb{M},k} = \left[ e^{-j2\pi \frac{(\mathbf{u}_1)^T \mathbf{b}_k}{c} f_c}, \dots, e^{-j2\pi \frac{(\mathbf{u}_M)^T \mathbf{b}_k}{c} f_c} \right]^T. \quad (8)$$

The AoA estimation method, i.e., MUSIC, can be applied to estimate  $(\varphi_k, \theta_k)$  using  $N$  snapshots of (7). However, when using  $\mathbf{r}_{\mathbb{M},n}$  to estimate AoAs directly, the number of resolvable signals is at most  $M - 1$ . To increase the DoFs and estimate more signals, a co-array is considered [25]. The covariance matrix  $\mathbf{R}_{\mathbb{M}}$  is derived from (7) as follows:

$$\begin{aligned} \mathbf{R}_{\mathbb{M}} &= \sum_{n=1}^N \mathbf{r}_{\mathbb{M},n} \mathbf{r}_{\mathbb{M},n}^H \\ &= \mathbf{A}_{\mathbb{M}} \begin{bmatrix} \sigma_1^2 & 0 & \dots & 0 \\ 0 & \sigma_2^2 & \dots & 0 \\ \vdots & \vdots & \ddots & \vdots \\ 0 & 0 & \dots & \sigma_K^2 \end{bmatrix} \mathbf{A}_{\mathbb{M}}^H + \mathbf{I}_M \sigma_0^2, \end{aligned} \quad (9)$$

where  $\mathbf{I}_M$  is an  $M$ -dimensional identity matrix and

$$\mathbf{A}_{\mathbb{M}} = [\mathbf{a}_{\mathbb{M},1}, \mathbf{a}_{\mathbb{M},2}, \dots, \mathbf{a}_{\mathbb{M},K}]. \quad (10)$$

Note that the second equation in (9) holds when the signals are uncorrelated. By vectorizing the covariance matrix  $\mathbf{R}_{\mathbb{M}}$  and ignoring the noise term, the following is obtained:

$$\begin{aligned} \text{vec}\{\mathbf{R}_{\mathbb{M}}\} &= \sum_{k=1}^K \sigma_k^2 \mathbf{a}_{\mathbb{M},k}^* \otimes \mathbf{a}_{\mathbb{M},k} \\ &= \sum_{k=1}^K \sigma_k^2 \mathbf{a}_{\mathbb{H},k}, \end{aligned} \quad (11)$$

where  $\mathbf{a}_{\mathbb{H},k} = \mathbf{a}_{\mathbb{M},k}^* \otimes \mathbf{a}_{\mathbb{M},k}$  denotes the steering vector for co-array  $\mathbb{H}$  and  $\text{vec}\{\mathbf{R}_{\mathbb{M}}\}$  can be viewed as a snapshot of the co-array located at  $\mathbb{H}$ , with

$$\begin{aligned} \mathbb{H} &= \{(i_h d, j_h d) | i_h = i_m - i_{m'}, j_h = j_m - j_{m'}, \\ &\quad (i_m d, j_m d) \in \mathbb{M}, (i_{m'} d, j_{m'} d) \in \mathbb{M}\}. \end{aligned} \quad (12)$$

By removing the repetitive elements in  $\mathbb{H}$ , the co-array location is derived as  $\tilde{\mathbb{H}}$ . Then, one snapshot of the co-array is derived from (11) as follows:

$$\mathbf{r}_{\tilde{\mathbb{H}}} = \sum_{k=1}^K \sigma_k^2 \mathbf{a}_{\tilde{\mathbb{H}},k}. \quad (13)$$

Sparsity-based methods, or spectral methods, can be used to estimate  $(\varphi_k, \theta_k)$  ( $1 \leq k \leq K$ ) in (13). For an array with

$M$  physical elements, the corresponding co-array has  $O(M^2)$  elements [25]. Most existing estimation methods assume a narrowband signal model. As the requirements related to the resolution or rate increase, the bandwidth of the signals progressively widens; thus, AoA estimation with broadband signals should be considered.

### III. AOA ESTIMATION OF BROADBAND SIGNALS USING NUPA

In this section, AoA estimation under a broadband signal model is analyzed. We propose the broadband co-array to enhance the AoA estimation performance. Moreover, to ensure adequate estimation performance in scenarios with fewer elements, an optimization method is proposed to improve the radiation pattern of the broadband co-array.

#### A. Analysis of the Broadband Co-array

An example is first presented to illustrate the benefits brought by broadband signals. Considering the space-domain samples of the  $m$ -th element at frequencies  $f_q$  and  $f_{q'}$  ( $f_{q'} > f_q$ ) as  $a_{m,k,q}$  and  $a_{m,k,q'}$ , respectively, the following is obtained:

$$a_{m,k,q'} = e^{-j2\pi \frac{f_{q'}/f_q [i_m d, j_m d] \mathbf{b}_k}{c}} f_q \quad (14)$$

It can be inferred from (3) that when  $(f_{q'} - f_q)^2 (i_m^2 + j_m^2) = f_q^2$ ,  $a_{m,k,q'}$  can be regarded as a space-domain sample of a virtual element  $d$  away from the  $m$ -th element. Thus, the broadband characteristics can be utilized to generate virtual elements to enhance the AoA estimation performance.

The analysis of a planar array receiving broadband signals yields the following theorem.

*Theorem 1:* Suppose that signals with bandwidth  $B$  and carrier frequency  $f_c$  are received by a planar array located at  $\mathbb{M} = \{(d i_m, d j_m)\}$  ( $1 \leq m \leq M$ ); a virtual array can be generated to increase the number of effective elements when there is at least one element in the array that satisfies  $\sqrt{i_m^2 + j_m^2} \geq 1/\eta - 0.5$ , where  $\eta = B/f_c$  denotes the relative bandwidth. The number of effective elements is at most  $M_{\text{virtual}}$ , where

$$M_{\text{virtual}} = M + \sum_{m=1}^M \left\lfloor \frac{2\eta \sqrt{i_m^2 + j_m^2}}{2 - \eta} \right\rfloor. \quad (15)$$

*Proof:* The proof is shown in Appendix A. ■

The condition  $\sqrt{i_m^2 + j_m^2} \geq 1/\eta - 0.5$  means that the maximum IES of the physical array should be larger than  $0.5c/B - 0.25c/f_c$ . A larger array size may lead to a reduction in the bandwidth. Under the above conditions, broadband signals can be exploited to increase the DoFs and thus enhance the estimation performance. In the extreme case where all the elements are far from reference element (0,0),  $M_{\text{virtual}}$  can nearly approach the value  $M + 4BMD_{\text{max}}/(2c - \eta c)$ , where  $D_{\text{max}}$  denotes the maximum IES.

As the array aperture, i.e.,  $\sqrt{i_m^2 + j_m^2}$ , or the relative bandwidth  $\eta$  increases, the number of virtual elements increases as well. From the proof in Appendix A, we can also find that the condition  $\sqrt{i_m^2 + j_m^2} \geq 1/\eta - 0.5$  requires the space samples at

distinct frequencies to be far enough apart, which means that the space samples of several narrow-band signals can also be used to formulate a virtual array.

Furthermore, with the generated virtual elements, a physical element and a virtual element, or two virtual elements, can be used to format an element pair with a small IES to perform Nyquist sampling in the space domain. Thus, the number of physical element pairs with small IESs is largely decreased to reduce mutual coupling. With the limited number of physical elements, physical elements are located far away from others to reduce mutual coupling and enlarge the aperture of the array, virtual elements which are generated from broadband signal and are usually located near physical elements help to resolve ambiguity in the angle domain.

A diagram of the signal model for the virtual array is presented in Fig. 1(b). The location of the virtual array is derived as follows:

$$\mathbb{V} = \{(i_v d, j_v d) | i_v = f_q i_m / f_1, j_v = f_q j_m / f_1, 1 \leq q \leq Q, (i_m d, j_m d) \in \mathbb{M}\}. \quad (16)$$

With the virtual array  $\mathbb{V}$ , the  $n$ -th snapshot  $\mathbf{r}_{\mathbb{V},n}$  is reformulated from (6) as follows:

$$\mathbf{r}_{\mathbb{V},n} = \sum_{k=1}^K \rho_{k,n} \mathbf{a}_{\mathbb{V},k} + \mathbf{n}_{\mathbb{V},n}, \quad (17)$$

where  $\mathbf{a}_{\mathbb{V},k}$  and  $\mathbf{n}_{\mathbb{V},n}$  represent the steering vector of the  $k$ -th signal and the noise at the  $n$ -th snapshot, respectively.

With  $N$  snapshots, the covariance matrix  $\mathbf{R}_{\mathbb{V}}$  is derived from (17) as follows:

$$\mathbf{R}_{\mathbb{V}} = \mathbf{E} \{ \mathbf{r}_{\mathbb{V},n} \mathbf{r}_{\mathbb{V},n}^H \} = \mathbf{A}_{\mathbb{V}} \begin{bmatrix} \sigma_1^2 & 0 & \cdots & 0 \\ 0 & \sigma_2^2 & \cdots & 0 \\ \vdots & \vdots & \ddots & \vdots \\ 0 & 0 & \cdots & \sigma_K^2 \end{bmatrix} \mathbf{A}_{\mathbb{V}}^H + \mathbf{I}_{|\mathbb{V}|} \sigma^2, \quad (18)$$

where  $\mathbf{I}_{|\mathbb{V}|}$  denotes the identity matrix of size  $|\mathbb{V}|$  and

$$\mathbf{A}_{\mathbb{V}} = [\mathbf{a}_{\mathbb{V},1}, \mathbf{a}_{\mathbb{V},2}, \cdots, \mathbf{a}_{\mathbb{V},K}]. \quad (19)$$

Note that the second equation in (18) holds when the signals are uncorrelated. By vectorizing the covariance matrix  $\mathbf{R}_{\mathbb{V}}$  and ignoring the noise term, the following is derived:

$$\begin{aligned} \text{vec} \{ \mathbf{R}_{\mathbb{V}} \} &= \sum_{k=1}^K \sigma_k^2 \mathbf{a}_{\mathbb{V},k}^* \otimes \mathbf{a}_{\mathbb{V},k} \\ &= \sum_{k=1}^K \sigma_k^2 \mathbf{a}_{\mathbb{W},k}, \end{aligned} \quad (20)$$

where  $\mathbf{a}_{\mathbb{W},k} = \mathbf{a}_{\mathbb{V},k}^* \otimes \mathbf{a}_{\mathbb{V},k}$  denotes the steering vector for broadband co-array  $\mathbb{W}$  and  $\text{vec} \{ \mathbf{R}_{\mathbb{V}} \}$  can be viewed as a snapshot of a broadband co-array located at  $\mathbb{W}$ , with

$$\mathbb{W} = \{(i_w d, j_w d) | i_w = i_v - i_{v'}, j_w = j_v - j_{v'}, (i_v d, j_v d) \in \mathbb{V}, (i_{v'} d, j_{v'} d) \in \mathbb{V}\}. \quad (21)$$

By removing the repetitive elements and the elements that are less than  $d$  away from some other element, the broadband

co-array location is derived from  $\mathbb{W}$  as  $\bar{\mathbb{W}}$ . Note that when two elements are less than  $d$  away from each other, we prefer to retain the one which is farther away from the reference element. Especially at the boundary of the array, the farther one helps to provide a larger aperture. Then, one snapshot of the broadband co-array is derived from (20) as follows:

$$\mathbf{r}_{\bar{\mathbb{W}}} = \sum_{k=1}^K \sigma_k^2 \mathbf{a}_{\bar{\mathbb{W}},k}. \quad (22)$$

In matrix form, (22) can be denoted as follows:

$$\mathbf{r}_{\bar{\mathbb{W}}} = \mathbf{A}_{\bar{\mathbb{W}}}\delta, \quad (23)$$

where  $\mathbf{A}_{\bar{\mathbb{W}}} = [\mathbf{a}_{\bar{\mathbb{W}},1}, \dots, \mathbf{a}_{\bar{\mathbb{W}},K}]$  and  $\delta = [\sigma_1^2, \dots, \sigma_K^2]^T$ .

Discretizing  $\varphi$  and  $\theta$  into  $N_\varphi$  and  $N_\theta$  grids, respectively, (23) can be expressed as follows:

$$\mathbf{r}_{\bar{\mathbb{W}}} = \bar{\mathbf{A}}_{\bar{\mathbb{W}}}\bar{\delta}, \quad (24)$$

where  $\bar{\mathbf{A}}_{\bar{\mathbb{W}}} = [\mathbf{a}_{\bar{\mathbb{W}},1,1}, \dots, \mathbf{a}_{\bar{\mathbb{W}},N_\varphi,N_\theta}]$  and  $\bar{\delta} = [\sigma_{1,1}^2, \dots, \sigma_{N_\varphi,N_\theta}^2]^T$ .  $\bar{\mathbf{A}}_{\bar{\mathbb{W}}}$  is an overcomplete dictionary with  $N_\varphi N_\theta$  columns, and  $\bar{\delta} = [\delta_{1,1}, \dots, \delta_{N_\varphi,N_\theta}]^T$  is a  $K$  sparse vector. Note that (24) is under the assumption that the  $(\varphi_k, \theta_k)$  ( $1 \leq k \leq K$ ) are located at the discrete grids  $(\varphi_{n_\varphi}, \theta_{n_\theta})$  ( $1 \leq n_\varphi \leq N_\varphi, 1 \leq n_\theta \leq N_\theta$ ). The AoA estimation is then transformed into the sparse recovery problem as follows:

$$\hat{\delta} = \arg \min_{\bar{\delta}} \|\bar{\delta}\|_0, \text{ s.t. } \mathbf{r}_{\bar{\mathbb{W}}} = \bar{\mathbf{A}}_{\bar{\mathbb{W}}}\bar{\delta}, \quad (25)$$

which can be solved by orthogonal matching pursuit [32] or other sparsity-based methods. When  $(\varphi_k, \theta_k)$  ( $1 \leq k \leq K$ ) are not exactly located at the discrete grids, some gridless methods [46], [47] can be used to improve the estimation performance. If multiple snapshots of (22) are available, some spectral methods, i.e. MUSIC [7], can be used to perform the estimation.

In contrast to existing studies, we generate the virtual array before generating the co-array. The generated virtual elements can substantially increase the number of elements in the co-array. As shown in Theorem 1, at most  $M_{\text{virtual}}$  effective virtual elements can be generated. Therefore, the corresponding co-array has at most  $\mathcal{O}(M_{\text{virtual}}^2)$  elements.

Analyzing the performance of the broadband co-array, the following theorem is given.

*Theorem 2:* Suppose that signals with bandwidth  $B$  and carrier frequency  $f_c$  are received by a planar array located at  $\mathbb{M} = \{(d_{i_m}, d_{j_m})\}$  ( $1 \leq m \leq M$ ); a virtual array can be generated to increase the number of effective elements in the co-array when there is at least one element pair  $(i_m d, j_m d)$  and  $(i_{m'} d, j_{m'} d)$ , satisfying the following:

$$\sqrt{(i_m + i_{m'})^2 + (j_m + j_{m'})^2} \geq \frac{1}{\eta} - 0.5. \quad (26)$$

*Proof:* The proof is shown in Appendix B. ■

Note that (26) can be simplified to  $2\sqrt{i_m^2 + j_m^2} \geq 1/\eta - 0.5$  when the IES of element pair  $(i_m d, j_m d)$  and  $(i_{m'} d, j_{m'} d)$  is much smaller than  $\sqrt{i_m^2 + j_m^2}$ . This means that the maximum IES of the physical array should be larger than  $0.25c/B -$

$0.125c/f_c$ . Comparing this condition with that in Theorem 1, we can find that the broadband co-array helps to release the constraint on the physical array size and further enlarges the benefit conferred by the virtual array.

The estimation performance is improved by generating much more elements offered by broadband co-array. Therefore, when some classical methods, i.e., spectral methods or sparsity-based methods, are applied to perform AoA estimation, the computational complexity increases in proportion to the elements offered by broadband co-array.

Analysis of the performance of the broadband co-array yields the following theorem.

*Theorem 3:* Suppose that signals with bandwidth  $B$  and carrier frequency  $f_c$  are received by a planar array located at  $\mathbb{M} = \{(d_{i_m}, d_{j_m})\}$  ( $1 \leq m \leq M$ ). The maximum IES at the X-axis and Y-axis is denoted as  $d_{i_{\max}}$  and  $d_{j_{\max}}$ , respectively. When  $\min(i_{\max}, j_{\max}) \geq 1/\eta - 0.5$  holds, the generated broadband co-array can enlarge the maximum IES at most to  $l_X$  and  $l_Y$  at the X-axis and Y-axis, respectively, where

$$\begin{aligned} l_X &= 2 \left( \left[ i_{\max} + \frac{2i_{\max}\eta}{2-\eta} \right] d, \right. \\ l_Y &= 2 \left( \left[ j_{\max} + \frac{2j_{\max}\eta}{2-\eta} \right] d. \right. \end{aligned} \quad (27)$$

*Proof:* The proof is shown in Appendix C. ■

The width of the main lobe of the radiation pattern is determined by the maximum IES, so it can be inferred from Theorem 3 that when applied to some existing 2D arrays, the broadband co-array can help to narrow the main lobe of the radiation pattern and promote the estimation performance. Moreover, as the relative bandwidth increases, the main lobe of the broadband co-array narrows.

## B. Array Design Method

In this subsection, the performance of the broadband co-array is employed as the metric to design the array. Among the studies focusing on designing arrays, some CRB-based methods [48], [49] have been proposed, but most of them are analyzed under the assumption of one signal, which may not be suitable in scenes with multiple signals. Some DoF-based methods [24], [25], [27] have also been proposed. However, we can infer from [50] that the AoA estimation performance depends not only on the DoFs but also on the performance of the manifold matrix of the co-array.

Considering the manifold matrix  $\mathbf{r}_{\bar{\mathbb{W}}} = \mathbf{A}_{\bar{\mathbb{W}}}\delta$  in (24), the maximum DoF offered extends to the number of rows of  $\mathbf{A}_{\bar{\mathbb{W}}}$ . Note that the maximum DoF is not suitable for arbitrary multiple signals. If  $\mathbf{A}_{\bar{\mathbb{W}}}$  is not full rank in a multi-signal scene, the corresponding CRB is not valid, and the estimation performance cannot be guaranteed [50].

We then consider both the DoFs and the performance of  $\mathbf{A}_{\bar{\mathbb{W}}}$  to design an array. Obviously, when the condition stated in Theorem 3 is satisfied, the broadband can help to increase the DoF. One way to increase the possibility that  $\mathbf{A}_{\bar{\mathbb{W}}}$  is full rank in a multi-signal scene is to decrease the coherence between steering vectors of two arbitrary signals. Some related results have been studied from the perspective of compressive

sensing [51], [52]. In compressive sensing, the Gram matrix of a dictionary is designed to approach the identity matrix as closely as possible for better performance [52]. As noted in the previous subsection, the AoA estimation can be transformed into a sparse recovery problem as in (24) and (25). Exploiting this, we can normalize the columns of dictionary  $\bar{\mathbf{A}}_{\bar{\mathbf{w}}}$  and optimize the array to make the Gram matrix of dictionary  $\bar{\mathbf{A}}_{\bar{\mathbf{w}}}^H \bar{\mathbf{A}}_{\bar{\mathbf{w}}}$  approach the identity matrix as closely as possible. Given the constrained size of the array  $i_{\max}$  and  $j_{\max}$ , four elements, i.e.,  $(0, 0)$ ,  $(di_{\max}, 0)$ ,  $(0, dj_{\max})$  and  $(di_{\max}, dj_{\max})$ , are first established to ensure the array aperture, and the other elements, with locations denoted as  $\mathbb{M}_1$ , are set by the following optimization problem:

$$\begin{aligned} \mathbb{M}_1 &= \arg \min_{\mathbb{M}_1} \left\| \mathbf{I} - \bar{\mathbf{A}}_{\bar{\mathbf{w}}}^H \bar{\mathbf{A}}_{\bar{\mathbf{w}}} \right\|_F^2 \\ \text{s.t. } &\begin{cases} 0 \leq i_m \leq i_{\max} \\ 0 \leq j_m \leq j_{\max} \end{cases} \end{aligned} \quad (28)$$

where  $\|\cdot\|_F^2$  denotes the Frobenius norm. It is difficult to derive the closed-form solution of (28). Some optimization method, i.e. a genetic algorithm (GA), can be used to solve (28). We also find that the optimization in (28) is equivalent to suppressing the sidelobes of the radiation pattern of the broadband co-array in all discrete directions.

#### IV. CRAMER-RAO BOUNDS

The CRB for the unconditional model was described in [43], but it is not suitable when the number of sources is larger than the number of elements. Research on the co-array was proposed in [50], which studied the CRB for 1-D AoA with a narrow-band signal.

We first extend the result in [50] to the CRB for a 2D AoA with a narrow-band signal and then derive the CRB for a 2D AoA with a broadband signal.

Given (6), the parameter vector is defined as follows:

$$\xi = [\xi_{\varphi, \theta}, \xi_{\sigma}]^T \quad (29)$$

with

$$\xi_{\varphi, \theta} = [\varphi_1, \theta_1, \dots, \varphi_K, \theta_K], \quad (30)$$

$$\xi_{\sigma} = [\sigma_1^2, \dots, \sigma_K^2, \sigma_0^2]. \quad (31)$$

The Fisher information matrix is then derived as follows [50]:

$$\text{FIM} = N \left[ \frac{\partial \mathbf{r}_{\mathbb{H}}}{\partial \xi} \right]^H (\mathbf{R}_{\mathbb{M}}^T \otimes \mathbf{R}_{\mathbb{M}})^{-1} \frac{\partial \mathbf{r}_{\mathbb{H}}}{\partial \xi}, \quad (32)$$

where

$$\frac{\partial \mathbf{r}_{\mathbb{H}}}{\partial \xi} = [\mathbf{A}_{\mathbb{H}} \mathbf{\Lambda}, \mathbf{A}_{\mathbb{H}}, \text{vec} \{ \mathbf{I}_M \}], \quad (33)$$

$$\mathbf{\Lambda} = \text{diag} \left( [\sigma_1^2, \sigma_1^2, \dots, \sigma_K^2, \sigma_K^2] \right), \quad (34)$$

$$\mathbf{A}_{\mathbb{H}} = \mathbf{A}_{\mathbb{M}}^* \odot \mathbf{A}_{\mathbb{M}} + \mathbf{A}_{\mathbb{M}}^* \odot \mathbf{A}_{\mathbb{M}}, \quad (35)$$

$$\mathbf{A}_{\mathbb{M}} = \left[ \frac{\partial \mathbf{a}_{\mathbb{M},1}}{\partial \varphi_1}, \frac{\partial \mathbf{a}_{\mathbb{M},1}}{\partial \theta_1}, \dots, \frac{\partial \mathbf{a}_{\mathbb{M},K}}{\partial \varphi_K}, \frac{\partial \mathbf{a}_{\mathbb{M},K}}{\partial \theta_K} \right], \quad (36)$$

$$\mathbf{A}_{\mathbb{H}} = [\mathbf{a}_{\mathbb{H},1}, \mathbf{a}_{\mathbb{H},2}, \dots, \mathbf{a}_{\mathbb{H},K}]. \quad (37)$$

Note that  $\mathbf{R}_{\mathbb{M}}$  is positive definite, so  $(\mathbf{R}_{\mathbb{M}}^T \otimes \mathbf{R}_{\mathbb{M}})^{-1}$  is positive definite and its square root  $(\mathbf{R}_{\mathbb{M}}^T \otimes \mathbf{R}_{\mathbb{M}})^{-1/2}$  exists. The partitioned Fisher information matrix is then derived as follows:

$$\text{FIM}_1 = N \begin{bmatrix} \mathbf{D}_{\mathbb{H},1}^H \mathbf{D}_{\mathbb{H},1} & \mathbf{D}_{\mathbb{H},1}^H \mathbf{D}_{\mathbb{H},2} \\ \mathbf{D}_{\mathbb{H},2}^H \mathbf{D}_{\mathbb{H},1} & \mathbf{D}_{\mathbb{H},2}^H \mathbf{D}_{\mathbb{H},2} \end{bmatrix}, \quad (38)$$

where

$$\mathbf{D}_{\mathbb{H},1} = (\mathbf{R}_{\mathbb{M}}^T \otimes \mathbf{R}_{\mathbb{M}})^{-1/2} \mathbf{A}_{\mathbb{H}} \mathbf{\Lambda}, \quad (39)$$

$$\mathbf{D}_{\mathbb{H},2} = (\mathbf{R}_{\mathbb{M}}^T \otimes \mathbf{R}_{\mathbb{M}})^{-1/2} [\mathbf{A}_{\mathbb{H}}, \text{vec} \{ \mathbf{I}_M \}]. \quad (40)$$

The CRB matrix for the 2D AoAs with narrowband signals is then derived by blockwise inversion from (38) as follows:

$$\text{CRB}_{\mathbb{H}, \varphi, \theta} = \frac{1}{N} \left( \mathbf{D}_{\mathbb{H},1}^H \mathbf{\Pi}_{\mathbb{H}}^{\perp} \mathbf{D}_{\mathbb{H},1} \right)^{-1}, \quad (41)$$

where  $\mathbf{\Pi}_{\mathbb{H}}^{\perp} = \mathbf{I}_{|\mathbb{H}|} - \mathbf{D}_{\mathbb{H},2} \left( \mathbf{D}_{\mathbb{H},2}^H \mathbf{D}_{\mathbb{H},2} \right)^{-1} \mathbf{D}_{\mathbb{H},2}^H$ .

With a broadband signal, the virtual array  $\mathbb{V}$  is first derived, and the samples of virtual array  $\mathbb{V}$  can be viewed as space domain samples at a single frequency. Therefore, we derive the CRB for a 2D AoA with a broadband signal following (41) as follows:

$$\text{CRB}_{\mathbb{W}, \varphi, \theta} = \frac{1}{N} \left( \mathbf{D}_{\mathbb{W},1}^H \mathbf{\Pi}_{\mathbb{W}}^{\perp} \mathbf{D}_{\mathbb{W},1} \right)^{-1}, \quad (42)$$

where

$$\mathbf{D}_{\mathbb{W},1} = (\mathbf{R}_{\mathbb{V}}^T \otimes \mathbf{R}_{\mathbb{V}})^{-1/2} \mathbf{A}_{\mathbb{W}} \mathbf{\Lambda}, \quad (43)$$

$$\mathbf{D}_{\mathbb{W},2} = (\mathbf{R}_{\mathbb{V}}^T \otimes \mathbf{R}_{\mathbb{V}})^{-1/2} [\mathbf{A}_{\mathbb{W}}, \text{vec} \{ \mathbf{I}_{|\mathbb{V}|} \}], \quad (44)$$

$$\mathbf{\Pi}_{\mathbb{W}}^{\perp} = \mathbf{I}_{|\mathbb{W}|} - \mathbf{D}_{\mathbb{W},2} \left( \mathbf{D}_{\mathbb{W},2}^H \mathbf{D}_{\mathbb{W},2} \right)^{-1} \mathbf{D}_{\mathbb{W},2}^H, \quad (45)$$

$$\mathbf{A}_{\mathbb{W}} = \mathbf{A}_{\mathbb{V}}^* \odot \mathbf{A}_{\mathbb{V}} + \mathbf{A}_{\mathbb{V}}^* \odot \mathbf{A}_{\mathbb{V}}, \quad (46)$$

$$\mathbf{A}_{\mathbb{V}} = \left[ \frac{\partial \mathbf{a}_{\mathbb{V},1}}{\partial \varphi_1}, \frac{\partial \mathbf{a}_{\mathbb{V},1}}{\partial \theta_1}, \dots, \frac{\partial \mathbf{a}_{\mathbb{V},K}}{\partial \varphi_K}, \frac{\partial \mathbf{a}_{\mathbb{V},K}}{\partial \theta_K} \right], \quad (47)$$

$$\mathbf{A}_{\mathbb{W}} = [\mathbf{a}_{\mathbb{W},1}, \mathbf{a}_{\mathbb{W},2}, \dots, \mathbf{a}_{\mathbb{W},K}]. \quad (48)$$

When the condition discussed in Theorem 1 is satisfied, the virtual array  $\mathbb{V}$  offers more elements than the physical array  $\mathbb{M}$ , and the lower CRB is acquired [43]. This indicates that the broadband signal can help to improve the CRB for a given array.

The element locations in the proposed array are obtained by optimization, and the closed-form locations can not be derived, so it is difficult to compare the CRB of the proposed array with that of other arrays mathematically. In the next section, the CRBs will be compared through simulation.

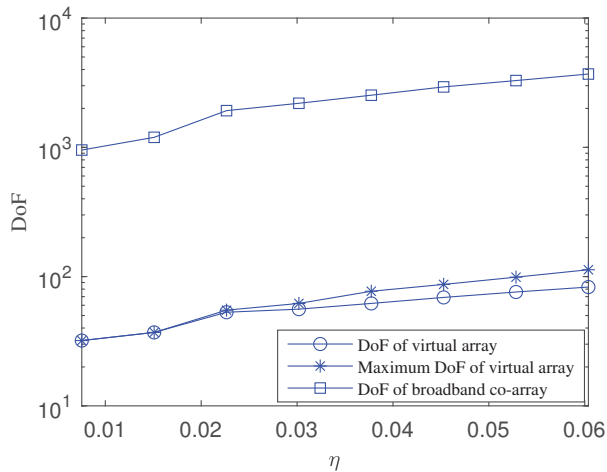


Fig. 2. DoFs of two kinds of arrays versus relative bandwidth.

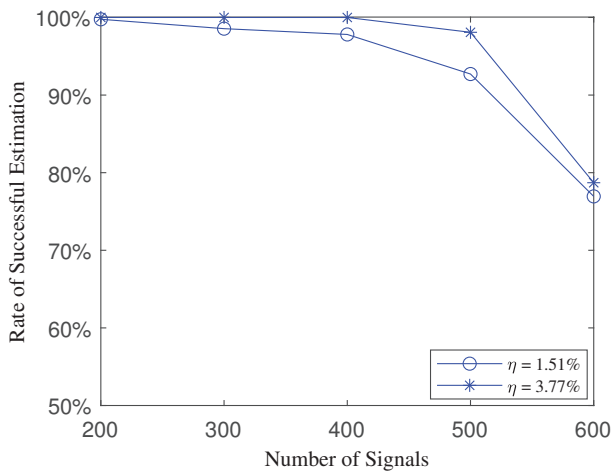


Fig. 3. Rate of successful estimations versus the number of signals for different bandwidths.

## V. NUMERICAL RESULTS

In this section, simulations are conducted to illustrate the AoA estimation performance using broadband signals and NUPA. The performance achieved by the designed NUPA is presented and then compared with that achieved by other methods. Some broadband signal-based methods, i.e., coherent signal subspace methods (CSSM) [38]–[40], have been thoroughly studied. However, the number of resolvable signals is still limited by the number of physical elements. Although the wideband DoA estimation with sparse linear arrays is studied in [42], Jacobi-Anger expansion, which plays a crucial role in the method, cannot be directly extended to 2D arrays. Therefore, the above methods are not considered the benchmark. We compare the performance achieved by the designed NUPA with that achieved by nested array [25]. In the simulations, the carrier frequency is set to  $f_c = 26.5$  GHz, which is used in millimeter-wave channel measurements. For Monte Carlo, five hundred trials are conducted. The co-arrays are generated from second-order statistics as in (18), and  $Q$  is set to be 5 for the broadband co-array. Both the sparsity-based method, i.e., OMP [32], and the spectral method, i.e., MUSIC [7],

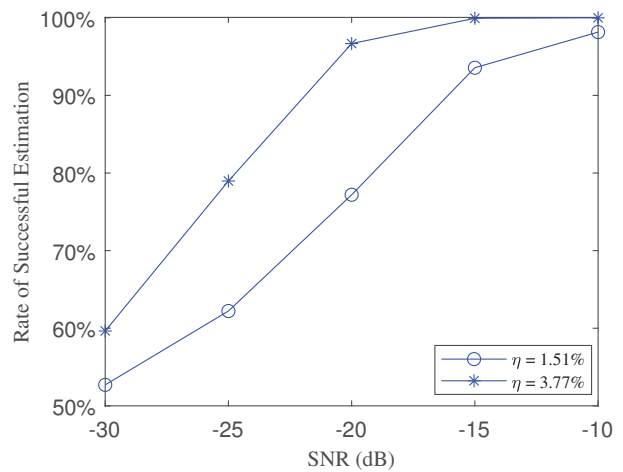


Fig. 4. Rate of successful estimation versus SNR for different bandwidths.

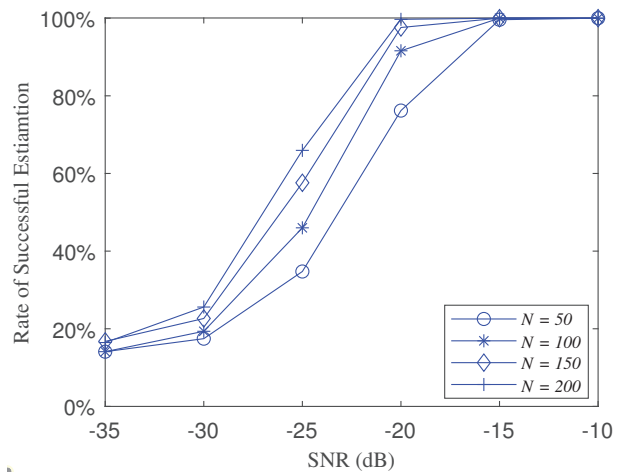


Fig. 5. Rate of successful estimation versus SNR for different numbers of snapshots.

are used to perform AoA estimation. OMP is conducted with one snapshot of the broadband co-array and its achievable resolution is closely correlated to the radiation pattern of the broadband co-array. It is difficult to be guaranteed to promote the estimation performance, even when the interval of discrete angle is too small. So we discretize the angle with the interval of  $5^\circ$ . When using OMP, the signals are assumed to be located at the discrete grids following a discrete uniform distribution in the range  $-60^\circ \sim 60^\circ$  for both the elevation angle and azimuth angle. The rate of successful estimation, where one successful estimation means that the estimated 2D-AoA is consistent with the set 2D-AoA, is taken as the performance metric for OMP. MUSIC is conducted with multiple snapshots of the broadband co-array and it can achieve super-resolution. The small search interval helps to promote the estimation performance. So the search interval is set to be  $0.2^\circ$ . When using MUSIC, both the elevation angle and azimuth angle of the signals are assumed to follow a uniform distribution in the range  $-60^\circ \sim 60^\circ$ . The root mean square error (RMSE) is taken as the performance

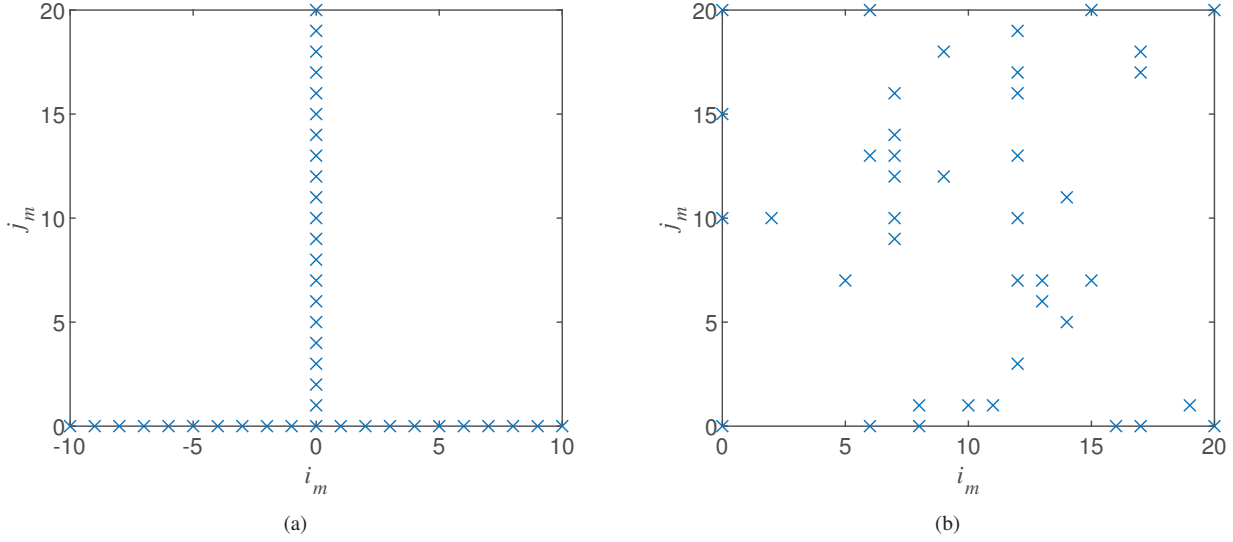


Fig. 6. The element locations of the physical array for different arrays: (a) Nested array; (b) NUPA.

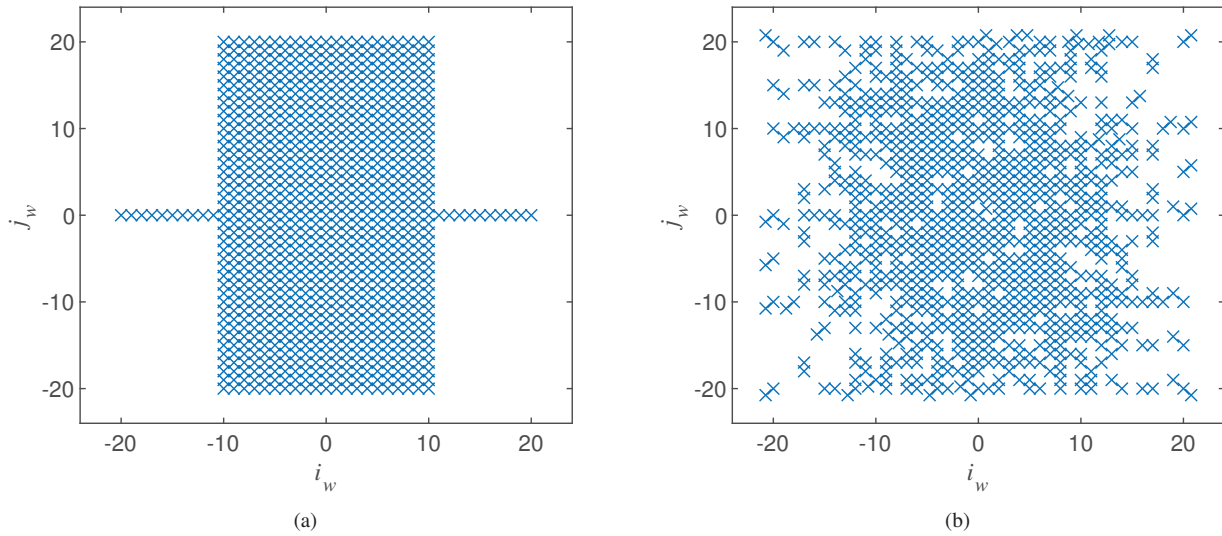


Fig. 7. The element locations of the co-array for different arrays: (a) Nested array; (b) NUPA.

metric and defined as follows:

$$\text{RMSE} = \text{E} \left\{ \left\| (\varphi, \theta) - (\hat{\varphi}, \hat{\theta}) \right\|_2 \right\}, \quad (49)$$

where  $(\hat{\varphi}, \hat{\theta})$  denotes the estimation of  $(\varphi, \theta)$ .

The robustness to mutual coupling is also simulated, where the entries of the mutual coupling matrix  $\langle \mathbf{C} \rangle_{m,m'}$  ( $1 \leq m, m' \leq M$ ) are set as

$$\langle \mathbf{C} \rangle_{m,m'} = \begin{cases} 1, & m = m', \\ 0.15, & 1 < \|(i_m, j_m) - (i_{m'}, j_{m'})\|_2 \leq 2, \\ 0.25, & 0 < \|(i_m, j_m) - (i_{m'}, j_{m'})\|_2 \leq 1, \\ 0, & \text{otherwise.} \end{cases} \quad (50)$$

The performance achieved by the designed NUPA is first presented. The DoFs of virtual arrays and broadband co-arrays versus relative bandwidth are shown in Fig. 2. The sizes of arrays  $i_{\max}$  and  $j_{\max}$  are both 60, and the number of elements

$M$  is 32. The axis of relative bandwidth extends from 0.75% to 6.04% with an interval of 0.75%, where the corresponding bandwidth axis is from 200 MHz to 1.6 GHz with an interval of 200 MHz. Obviously, the broadband signal helps to largely increase the DoFs of both virtual arrays and broadband co-arrays as the relative bandwidth increases. In the case of 200 MHz, when the condition in Theorem 1 is not satisfied, the number of DoFs of the virtual array remains 32. When the bandwidth reaches 400 MHz, the condition is satisfied, and the DoFs increase to 37. As shown in Fig. 2, the DoFs of the virtual array are limited by  $M_{\text{virtual}}$  as (15), and the corresponding increasing rate versus the relative bandwidth is less than that of  $M_{\text{virtual}}$ . As the relative bandwidth increases, more virtual elements are generated, which leads to many element pairs with IESs less than  $d$ . Therefore, some of the generated virtual elements are removed as noneffective elements. It is known that the co-array of a physical array

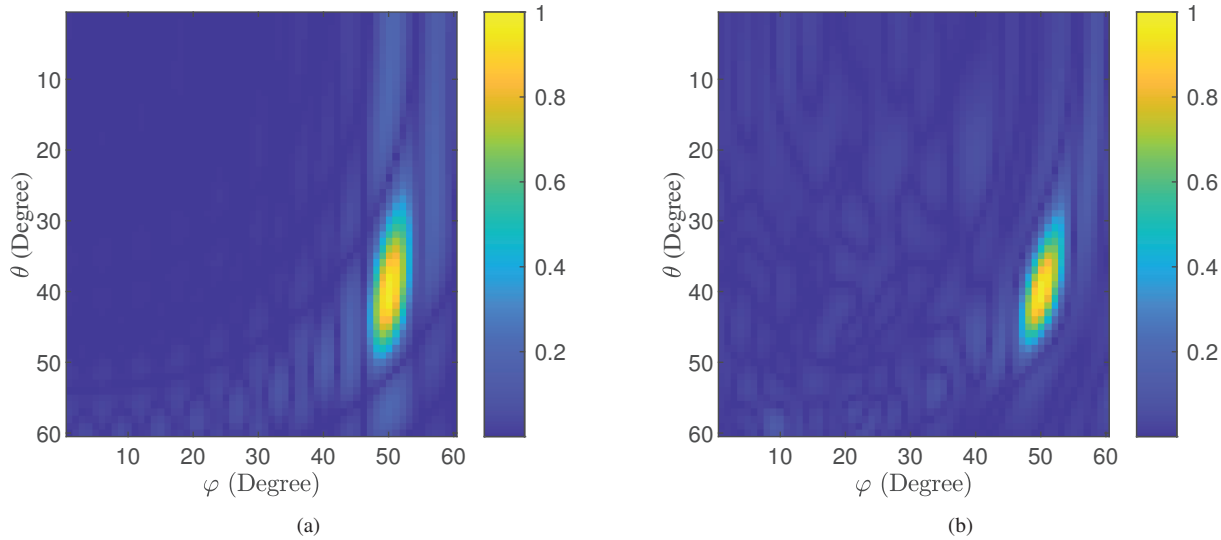


Fig. 8. The co-array radiation patterns for different arrays: (a) Nested array; (b) NUPA.

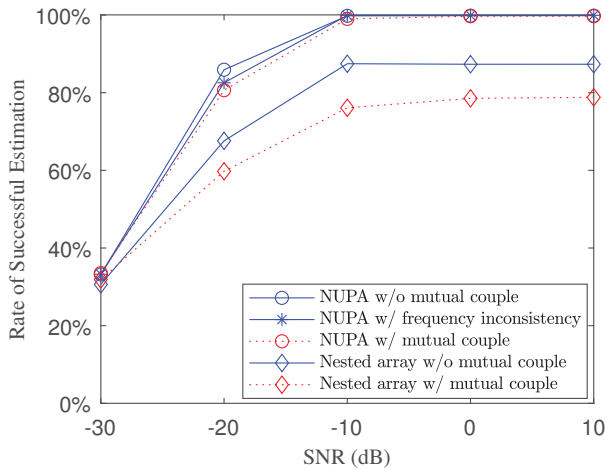


Fig. 9. Rate of successful estimation versus SNR for different arrays.

with 32 elements offers a DoF limit of 1,024. We can see from Fig. 2 that the DoFs offered by broadband co-array surpass twice the limit even with a relative bandwidth of 2.26%. Furthermore, the increasing rate of DoFs offered by the broadband co-array is larger than that offered by the virtual array, which indicates that the broadband co-array can further enhance the benefit produced by the virtual array.

The estimation performance with different bandwidths is compared. The situation where only one snapshot of (23) is available is first considered. Therefore, OMP is used to perform the AoA estimation, and the rate of successful estimation is taken as the metric. The  $N$  value is set to 700. Note that setting a high value of  $N$  is used to guarantee the performance when solving several hundred signals. When several signals are present, the value of  $N$  can be set to a small number. The rate of successful estimation versus the number of signals is shown in Fig. 3 when the SNR is -5 dB. A larger relative bandwidth ( $\eta = 3.77\%$ ) leads to more DoFs and, thus, helps to solve more signals. Although  $\eta = 3.77\%$  can offer 2,531 DoFs,

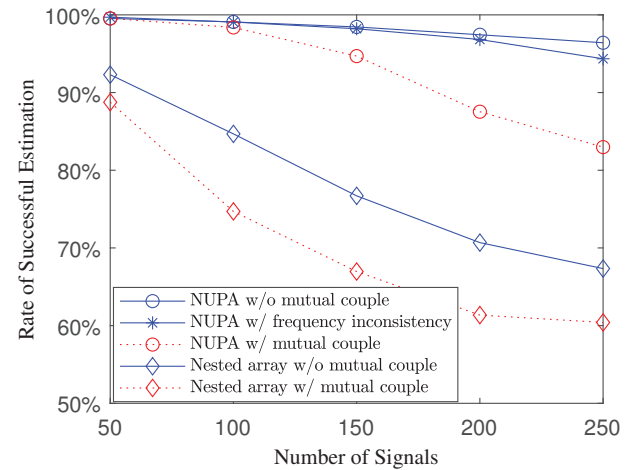


Fig. 10. Rate of successful estimations versus the number of signals for different arrays.

as shown in Fig. 2, the estimation performance decreases when the number of signals exceeds 400. This is because the maximum DoF value is not suitable for arbitrary multiple signals, and the manifold matrix of the co-array should be guaranteed to be full rank. The rate of successful estimation versus SNR is shown in Fig. 4 when the number of signals is 300. As shown in Fig. 2,  $\eta = 3.77\%$  and  $\eta = 1.5\%$  can increase the effective elements of the co-array to 2,531 and 1,195, respectively. A large number of effective elements can also help to increase the robustness to noise.

The estimation performance for different numbers of snapshots is presented in Fig. 5, where the number of signals is 40 and  $\eta = 3.77\%$ . All snapshot numbers are set to be larger than the number of signals to ensure that the manifold matrix of the broadband co-array is full rank. More snapshots lead to enhanced robustness performance. It can be inferred that the required number of snapshots needs only to be larger than the number of signals to guarantee the performance for practical

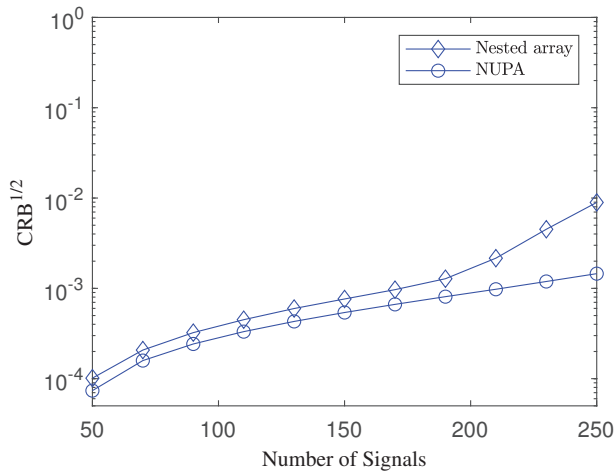


Fig. 11. CRB versus the number of signals for different arrays.

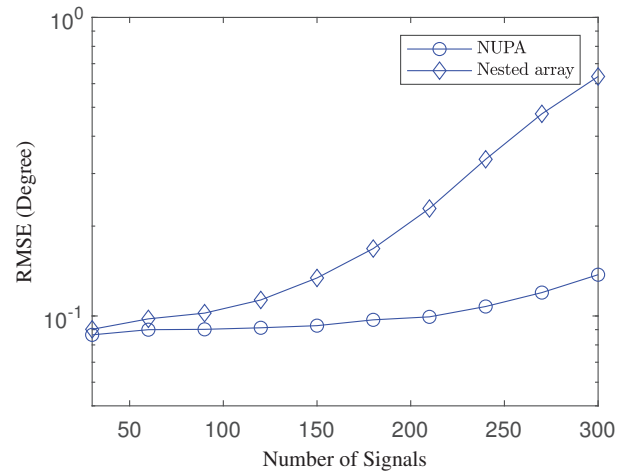


Fig. 12. RMSE versus number of signals for different arrays, where SNR = 20 dB.

deployment.

The performance achieved by the designed NUPA is then compared with that achieved by the nested array. The bandwidth is set to  $B = 1$  GHz. A nested array with 41 elements is generated according to [25], and an NUPA with 41 elements is generated by a GA. To maintain the same aperture as the nested array, we set  $i_{\max} = 20$  and  $j_{\max} = 20$ .

The element locations of the two arrays are presented in Fig. 6. Compared with the nested array, the NUPA has much fewer element pairs with IESs less than  $2d$ . The details are shown in Table V, where the NUPA has only 25 element pairs with IESs less than  $2d$ . This finding confirms that the virtual array leads to fewer element pairs with small IESs to reduce mutual coupling. The corresponding co-arrays and the radiation patterns on  $(50^\circ, 40^\circ)$  are shown in Fig. 7 and Fig. 8, respectively. As shown in Fig. 7, the broadband signal can help to enlarge the aperture of the co-array. Owing to the larger aperture and the optimization as (28), the NUPA can achieve a better radiation pattern with a narrower main lobe and lower side lobes.

The estimation performance with one snapshot of the co-array for the two arrays is compared in Fig. 9 and Fig. 10, where the rate of successful estimation versus SNR is shown in Fig. 9 when the number of signals is 100 and the rate versus the number of signals is shown in Fig. 10 when the SNR is 10 dB. The  $N$  is set to 300. When the bandwidth is too wide, the reflection coefficient may vary with the frequency slightly. We consider the coefficient inconsistency at different frequencies and set the maximum inconsistency of power to 3 dB. The robustness to mutual coupling is also compared,

TABLE I  
PERFORMANCE COMPARISONS OF THE PROPOSED NUPA WITH THE NESTED ARRAY.

Array type	DoFs of Co-array	Number of element pairs with IES less than $2d$
Nested array	881	80
NUPA	925	25

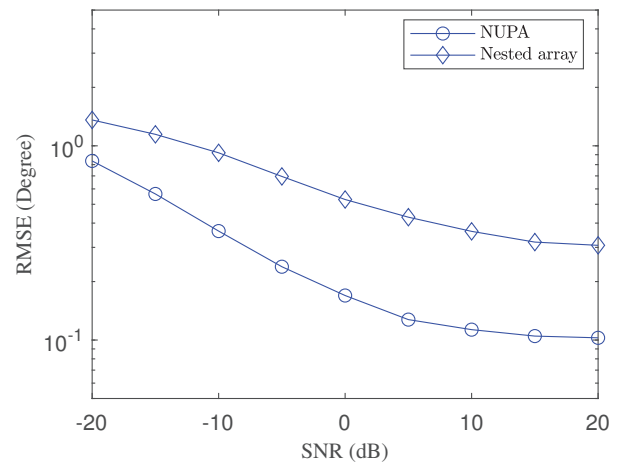


Fig. 13. RMSE versus SNR for different arrays, where the number of signals is 200.

and the model is set as previously defined. Similar to the comparisons of DoFs and radiation patterns, the rate achieved by the NUPA outperforms that achieved by the nested array in Fig. 9. More effective elements and fewer element pairs with small IESs, as shown in Table I, make the NUPA more robust to noise and mutual coupling. Note that the nested array cannot resolve 100 signals with rate 100% even when the SNR exceeds 10 dB. Although the co-array generated from the nested array can offer 881 DoFs, as shown in Table I, the manifold matrix of the co-array is not always guaranteed to be full rank when many signals are present. This may decrease the estimation performance. We find that the coefficient inconsistency at different frequencies has only a minimal effect on the performance achieved by NUPA. As shown in Fig. 10, the designed NUPA can solve 200 signals even with only 41 physical elements, while the nested array cannot always guarantee the estimation performance when many signals are present.

The two arrays are then compared in the situation where  $N$  is set to 400, and 400 snapshots of (23) are available.

A large number of snapshots of (23) is set to guarantee the performance when solving several hundred signals using MUSIC, and the number can be set low when several signals are present. As discussed in [50], the CRBs for co-arrays work well when the SNR is sufficiently high. This means that it is more suitable to compare CRBs versus the number of signals. The CRBs of NUPA and the nested array are shown in Fig. 11. Even though the CRB of the co-array cannot cover the entire range of SNRs, it somewhat confirms the superior performance of NUPA over the nested array.

The estimation performance results by MUSIC are shown in Fig. 12 and Fig. 13. Fig. 12 shows the RMSE versus the number of signals when the SNR is 20 dB. As the number of signals increases, the performance achieved by the nested array rapidly decreases, while the RMSE achieved by NUPA approaches  $0.1^\circ$  even when the number of signals exceeds 200. The result is consistent with that shown in Fig. 10. Fig. 13 illustrates the RMSE versus SNR when the number of signals is 200. We find that the RMSE achieved by the nested array remains  $0.5^\circ$  even when the search interval is  $0.2^\circ$  and the SNR approaches 20 dB. This further verifies the effectiveness of the proposed NUPA.

## VI. CONCLUSION

AOA estimation of broadband signals using NUPA has been considered in this work. A broadband co-array has been proposed to enhance the estimation performance from the perspective of mutual coupling, DoFs and CRB. The analysis of the relationship between frequency-domain samples and space-domain samples has indicated that the generated virtual array not only reduces mutual coupling but also increases the DoFs of the broadband co-array. We have also verified that the CRB can be improved with the help of broadband signals. To ensure adequate estimation performance in scenarios with fewer elements, an optimization method has been proposed to improve the performance of the broadband co-array.

### APPENDIX A PROOF OF THEOREM 1

The space domain samples of the  $m$ -th element at frequencies  $f_q$  and  $f_{q'}$  ( $f_{q'} > f_q$ ) are denoted as  $a_{m,k,q}$  and  $a_{m,k,q'}$ , respectively. According to (3),  $a_{m,k,q'}$  can be equivalent to a space-domain sample of virtual element  $[f_{q'}/f_q i_m d, f_{q'}/f_q j_m d]$ . When space sampling is performed, it is assumed that only the virtual element that is at least  $d$  away from others does not oversample and is considered an effective virtual element. Therefore, to generate effective virtual elements, it is expected that

$$\left(\frac{f_{q'}}{f_q} i_m d - i_m d\right)^2 + \left(\frac{f_{q'}}{f_q} j_m d - j_m d\right)^2 \geq d^2. \quad (51)$$

Simplification of (51) yields the following:

$$(f_{q'} - f_q)^2 (i_m^2 + j_m^2) \geq f_q^2. \quad (52)$$

Note that  $f_q$  and  $f_{q'}$  are constrained as follows:

$$f_c - \frac{B}{2} \leq f_q < f_{q'} \leq f_c + \frac{B}{2}. \quad (53)$$

By substituting (53) into (52), it is derived that

$$\begin{aligned} \sqrt{i_m^2 + j_m^2} &\geq \frac{2f_c - B}{2B} \\ &= \frac{1}{\eta} - 0.5. \end{aligned} \quad (54)$$

Thus, a virtual array can be generated to increase the number of effective elements when there is at least one element in array  $(i_m d, j_m d)$  that satisfies  $\sqrt{i_m^2 + j_m^2} \geq 1/\eta - 0.5$ .

Denoting  $M_m$  as the number of virtual elements generated by the  $m$ -th element, it can be directly derived from (54) that  $M_m$  satisfies the following:

$$M_m \leq \left\lfloor \frac{2B\sqrt{i_m^2 + j_m^2}}{2f_c - B} \right\rfloor. \quad (55)$$

For an array with  $M$  elements, the total number of elements in the virtual array satisfies the following:

$$\begin{aligned} M + \sum_{m=1}^M M_m &\leq M + \sum_{m=1}^M \left\lfloor \frac{2B\sqrt{i_m^2 + j_m^2}}{2f_c - B} \right\rfloor \\ &= M + \sum_{m=1}^M \left\lfloor \frac{2\eta\sqrt{i_m^2 + j_m^2}}{2 - \eta} \right\rfloor. \end{aligned} \quad (56)$$

### APPENDIX B PROOF OF THEOREM 2

The generation of broadband co-arrays can be viewed as operations on space samples at distinct frequencies. To simplify the analysis, we take the space samples from the  $m$ -th element and  $m'$ -th element at  $f_q$  and  $f_{q'}$ , respectively. Without loss of generality, it is assumed that  $f_{q'} > f_q$ ,  $(i_{m'} + j_{m'})^2 > (i_m + j_m)^2$  and  $(i_{m'} - i_m)^2 + (j_{m'} - j_m)^2 \geq 1$ . Therefore, the corresponding virtual array  $\mathbb{V}'$  is derived as follows:

$$\mathbb{V}' = \left\{ \left( \frac{f_{q'}}{f_q} i_m d, \frac{f_{q'}}{f_q} j_m d \right), \left( \frac{f_{q'}}{f_q} i_{m'} d, \frac{f_{q'}}{f_q} j_{m'} d \right), (i_{m'} d, j_{m'} d), (i_m d, j_m d) \right\} \quad (57)$$

The location of broadband co-array  $\mathbb{W}'$  is then derived as follows:

$$\mathbb{W}' = \{(i_w d, j_w d) | i_w = i_v - i_{v'}, j_w = j_v - j_{v'}, (i_v d, j_v d) \in \mathbb{V}', (i_{v'} d, j_{v'} d) \in \mathbb{V}'\}. \quad (58)$$

If only the space samples at frequency  $f_q$  are considered, the location of co-array  $\mathbb{H}'$  is derived as follows:

$$\mathbb{H}' = \{(i_m d, j_m d), (i_{m'} d, j_{m'} d), (i_m d - i_{m'} d, j_m d - j_{m'} d), (i_{m'} d - i_m d, j_{m'} d - i_m d)\}. \quad (59)$$

Note that the elements increased by the co-array are centrosymmetric. In  $\mathbb{H}'$ , the number of increased elements by the co-array is 2, and there is 1 increased element on each side. Similarly, in  $\mathbb{W}'$ , the number of increased elements by the broadband co-array is 12, and there are 6 increased elements on each side. The element pairs with maximum interelement spacing on the positive side can be derived from (57) as follows:

$$(i_w d, j_w d) = \left( \left( i_{m'} - \frac{f_{q'}}{f_q} i_m \right) d, \left( j_{m'} - \frac{f_{q'}}{f_q} j_m \right) d \right), \quad (60)$$

$$(i_{w'd}, j_{w'd}) = \left( \left( \frac{f_{q'}}{f_q} i_{m'} - i_m \right) d, \left( \frac{f_{q'}}{f_q} j_{m'} - j_m \right) d \right). \quad (61)$$

Comparing  $\mathbb{W}'$  with  $\mathbb{H}'$ , if the virtual elements help to generate more effective elements in the broadband co-array, there should be at least 2 effective elements among 6 increased elements on each side. It is expected that the interelement spacing between  $(i_w d, j_w d)$  and  $(i_{w'} d, j_{w'} d)$  is larger than  $d$  to ensure at least 2 effective elements, so the following is derived:

$$\sqrt{(i_w d - i_{w'} d)^2 + (j_w d - j_{w'} d)^2} \geq d. \quad (62)$$

Simplification of (62) yields the following:

$$\sqrt{(i_{m'} + i_m)^2 + (j_{m'} + j_m)^2} \geq \frac{f_q}{f_{q'} - f_q}. \quad (63)$$

Note that  $f_q$  and  $f_{q'}$  are constrained as (53). Substituting (53) into (63) yields the following:

$$\begin{aligned} \sqrt{(i_{m'} + i_m)^2 + (j_{m'} + j_m)^2} &\geq \frac{2f_c - B}{2B} \\ &= \frac{1}{\eta} - 0.5. \end{aligned} \quad (64)$$

Thus, a virtual array can be generated to increase the number of effective elements in the co-array when there is at least one element pair  $(i_m d, j_m d)$  and  $(i_{m'} d, j_{m'} d)$  satisfying (64).

#### APPENDIX C PROOF OF THEOREM 3

It can be derived from (55) that when  $i_{\max} \geq (2f_c - B)/(2B)$  holds, the corresponding element can generate  $2Bi_{\max}/(2f_c - B)$  virtual elements, so the maximum IES of the virtual array at the X-axis is derived as  $(\lfloor i_{\max} + 2i_{\max}B/(2f_c - B) \rfloor)d$ . According to the principles used in generating the co-array, the maximum IES of the broadband co-array at the X-axis is twice that of the virtual array and is derived as follows:

$$\begin{aligned} l_X &= 2 \left( \left\lfloor i_{\max} + \frac{2i_{\max}B}{2f_c - B} \right\rfloor \right) d \\ &= 2 \left( \left\lfloor i_{\max} + \frac{2i_{\max}\eta}{2 - \eta} \right\rfloor \right) d. \end{aligned} \quad (65)$$

The same results can be derived at the Y-axis, i.e., the maximum IES of the broadband co-array at the Y-axis is as follows:

$$l_Y = 2 \left( \left\lfloor j_{\max} + \frac{2j_{\max}\eta}{2 - \eta} \right\rfloor \right) d. \quad (66)$$

Therefore, when  $\min(i_{\max}, j_{\max}) \geq (2f_c - B)/(2B)$  holds, the generated broadband co-array can enlarge the maximum IES to at most  $l_X$  and  $l_Y$  at the X-axis and Y-axis, respectively.

#### REFERENCES

- [1] E. G. Larsson, O. Edfors, F. Tufvesson, and T. L. Marzetta, "Massive MIMO for next generation wireless systems," *IEEE Commun. Mag.*, vol. 52, no. 2, pp. 186–195, Feb. 2014.
- [2] J. Lee, G. Gil, and Y. H. Lee, "Channel estimation via orthogonal matching pursuit for hybrid mimo systems in millimeter wave communications," *IEEE Trans. Commun.*, vol. 64, no. 6, pp. 2370–2386, Jun. 2016.
- [3] M. I. Skolnik, *Introduction to Radar Systems, 3rd ed.* McGraw Hill, 2001.

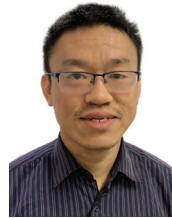
- [4] Y. Wang and K. C. Ho, "Unified near-field and far-field localization for AOA and hybrid AOA-TDOA positionings," *IEEE Trans. Wireless Commun.*, vol. 17, no. 2, pp. 1242–1254, Feb. 2018.
- [5] B. Yang, P. Zhang, H. Wang, C. X. Wang, and X. You, "Broadband extended array response-based subspace multiparameter estimation method for multipolarized wireless channel measurements," *IEEE Trans. Commun.*, 2021.
- [6] C. X. Wang, J. Huang, H. Wang, X. Gao, X. You, and Y. Hao, "6G wireless channel measurements and models: Trends and challenges," *IEEE Veh. Technol. Mag.*, vol. 15, no. 4, pp. 22–32, Dec. 2020.
- [7] R. Schmidt, "Multiple emitter location and signal parameter estimation," *IEEE Trans. Antennas Propag.*, vol. 34, no. 3, pp. 276–280, Mar. 1986.
- [8] R. Roy and T. Kailath, "ESPRIT-estimation of signal parameters via rotational invariance techniques," *IEEE Trans. Acoust., Speech, Signal Process.*, vol. 37, no. 7, pp. 984–995, Jul. 1989.
- [9] B. Friedlander, "The root-MUSIC algorithm for direction finding with interpolated arrays," *Signal Process.*, vol. 30, pp. 15–29, 1993.
- [10] M. D. Zoltowski, M. Haardt, and C. P. Mathews, "Closed-form 2-D angle estimation with rectangular arrays in element space or beamspace via unitary ESPRIT," *IEEE Trans. Signal Process.*, vol. 44, no. 2, pp. 316–328, Feb. 1996.
- [11] X. Dai, X. Zhang, and Y. Wang, "Extended DOA-matrix method for DOA estimation via two parallel linear arrays," *IEEE Commun. Lett.*, vol. 23, no. 11, pp. 1981–1984, Nov. 2019.
- [12] F. Shu, Y. Qin, T. Liu, L. Gui, Y. Zhang, J. Li, and Z. Han, "Low-complexity and high-resolution DOA estimation for hybrid analog and digital massive MIMO receive array," *IEEE Trans. Commun.*, vol. 66, no. 6, pp. 2487–2501, Jun. 2018.
- [13] P. Stoica and A. Nehorai, "MUSIC, maximum likelihood, and Cramer-Rao bound," *IEEE Trans. Acoust., Speech, Signal Process.*, vol. 37, no. 5, pp. 720–741, May 1989.
- [14] B. Friedlander, A. Friedlander, and A. Weiss, "Direction finding in the presence of mutual coupling," *IEEE Trans. Antennas Propag.*, vol. 39, no. 3, pp. 273–284, Mar. 1991.
- [15] C. A. Balanis, *Antenna Theory: Analysis and Design, 4th ed.* Hoboken, NJ, USA: Wiley, 2016.
- [16] J. Wallace and M. Jensen, "Mutual coupling in MIMO wireless systems: a rigorous network theory analysis," *IEEE Trans. Wireless Commun.*, vol. 3, no. 4, pp. 1317–1325, Jul. 2004.
- [17] Y. D. Zhang, M. G. Amin, and B. Himed, "Sparsity-based DOA estimation using coprime arrays," in *Proc. IEEE Int. Conf. Acoust. Speech Signal Process. (ICASSP)*, Vancouver, Canada, May. 2005, pp. 3967–3971.
- [18] P. P. Vaidyanathan and P. Pal, "Sparse sensing with coprime samplers and arrays," *IEEE Trans. Signal Process.*, vol. 59, no. 2, pp. 573–586, Feb. 2011.
- [19] A. T. Moffet, "Minimum-redundancy linear arrays," *IEEE Trans. Antennas Propag.*, vol. 16, no. 2, pp. 172–175, Mar. 1968.
- [20] P. Pal and P. P. Vaidyanathan, "Nested arrays: A novel approach to array processing with enhanced degrees of freedom," *IEEE Trans. Signal Process.*, vol. 58, no. 8, pp. 4167–4181, Aug. 2010.
- [21] C.-L. Liu and P. P. Vaidyanathan, "Super nested arrays: Linear sparse arrays with reduced mutual coupling Part I: Fundamentals," *IEEE Trans. Signal Process.*, vol. 64, no. 15, pp. 3997–4012, Aug. 2016.
- [22] J. Wang, H. Xu, G. J. T. Leus, and G. A. E. Vandenbosch, "Experimental assessment of the co-array concept for DOA estimation in wireless communications," *IEEE Trans. Antennas Propag.*, vol. 66, no. 6, pp. 3064–3075, June 2018.
- [23] J. Shi, G. Hu, X. Zhang, and H. Zhou, "Sparsity-based 2-D DOA estimation for co-prime array: from sum-difference co-array viewpoint," *IEEE Trans. Signal Process.*, vol. 65, no. 21, pp. 5591–5604, Nov. 2017.
- [24] C.-L. Liu and P. P. Vaidyanathan, "Hourglass arrays and other novel 2-D sparse arrays with reduced mutual coupling," *IEEE Trans. Signal Process.*, vol. 65, no. 13, pp. 3369–3383, July 2017.
- [25] P. Pal and P. P. Vaidyanathan, "Nested arrays in two dimensions, Part II: Application in two dimensional array processing," *IEEE Trans. Signal Process.*, vol. 60, no. 9, pp. 4706–4718, Sep. 2012.
- [26] Q. Wu, F. Sun, P. Lan, and G. Ding, "Two-dimensional direction of arrival estimation for co-prime planar arrays: a partial spectral search approach," *IEEE Sensors J.*, vol. 16, no. 14, pp. 5660–5670, Jul. 2016.
- [27] P. Pal and P. P. Vaidyanathan, "Nested arrays in two dimensions, Part I: Geometrical considerations," *IEEE Trans. Signal Process.*, vol. 60, no. 9, pp. 4694–4705, Sep. 2012.
- [28] R. A. Haubrich, "Array design," *Bull. Seismol. Soc. Amer.*, vol. 58, no. 3, pp. 977–991, Jun. 1968.
- [29] C. R. Greene and R. C. Wood, "Sparse array performance," *J. Acoust. Soc. Amer.*, vol. 63, no. 6, pp. 1866–1872, 1978.

- [30] D. L. Donoho, "Compressed sensing," *IEEE Trans. Inf. Theory*, vol. 52, no. 4, pp. 1289–1306, May 2006.
- [31] R. G. Baraniuk, "Compressive sensing," *IEEE Signal Process. Mag.*, vol. 24, no. 4, pp. 118–121, July 2007.
- [32] J. A. Tropp and A. C. Gilbert, "Signal recovery from random measurements via orthogonal matching pursuit," *IEEE Trans. Inf. Theory*, vol. 53, no. 12, pp. 4655–4666, Dec. 2007.
- [33] J. Li, Y. Li, and X. Zhang, "Two-dimensional off-grid DOA estimation using unfolded parallel coprime array," *IEEE Commun. Lett.*, vol. 22, no. 12, pp. 2495–2498, Dec. 2018.
- [34] Z. Zheng and S. Mu, "Two-dimensional DOA estimation using two parallel nested arrays," *IEEE Commun. Lett.*, vol. 24, no. 3, pp. 568–571, Mar. 2020.
- [35] J. Li, D. Jiang, and X. Zhang, "DOA estimation based on combined unitary ESPRIT for coprime MIMO radar," *IEEE Commun. Lett.*, vol. 21, no. 1, pp. 96–99, Jan. 2017.
- [36] C. Zhou, Y. Gu, X. Fan, Z. Shi, G. Mao, and Y. D. Zhang, "Direction-of-arrival estimation for coprime array via virtual array interpolation," *IEEE Trans. Signal Process.*, vol. 66, no. 22, pp. 5956–5971, Nov. 2018.
- [37] X. You, C. Wang, J. Huang, and et al., "Towards 6G wireless communication networks: Vision, enabling technologies, and new paradigm shifts," *Sci. China Inf. Sci.*, vol. 64, 2021.
- [38] H. Wang and M. Kaveh, "Coherent signal-subspace processing for the detection and estimation of angles of arrival of multiple wide-band sources," *IEEE Trans. Acoust., Speech, Signal Process.*, vol. 33, no. 4, pp. 823–831, Aug. 1985.
- [39] H. Hung and M. Kaveh, "Focussing matrices for coherent signal subspace processing," *IEEE Trans. Acoust., Speech, Signal Process.*, vol. 36, no. 8, pp. 1272–1281, Aug. 1988.
- [40] T.-S. Lee, "Efficient wideband source localization using beamforming invariance technique," *IEEE Trans. Signal Process.*, vol. 42, no. 6, pp. 1376–1387, Jun. 1994.
- [41] D. Swingler and J. Krolik, "Source location bias in the coherently focused high-resolution broadband beamformer," *IEEE Trans. Acoust., Speech, Signal Process.*, vol. 37, no. 1, pp. 143–145, Jan. 1989.
- [42] F. Wang, Z. Tian, G. Leus, and J. Fang, "Direction of arrival estimation of wideband sources using sparse linear arrays," *IEEE Trans. Signal Process.*, 2021.
- [43] P. Stoica and A. Nehorai, "Performance study of conditional and unconditional direction-of-arrival estimation," *IEEE Trans. Acoust., Speech, Signal Process.*, vol. 38, no. 10, pp. 1783–1795, Oct. 1990.
- [44] Y. Li, K. Lee, and Y. Bresler, "Optimal sample complexity for blind gain and phase calibration," *IEEE Trans. Signal Process.*, vol. 64, no. 21, pp. 5549–5556, Nov. 2016.
- [45] Y. Li and K. Lee, "Blind gain and phase calibration via sparse spectral methods," *IEEE Trans. Inf. Theory*, vol. 65, no. 5, pp. 3097–3123, May 2019.
- [46] K. Fyhn, M. Duarte, and S. Holdt Jensen, "Compressive parameter estimation for sparse translation-invariant signals using polar interpolation," *IEEE Trans. Signal Process.*, vol. 63, no. 4, pp. 870–881, Feb. 2015.
- [47] Z. Yang and L. Xie, "On gridless sparse methods for line spectral estimation from complete and incomplete data," *IEEE Trans. Signal Process.*, vol. 63, no. 12, pp. 3139–3153, Jun. 2015.
- [48] H. Gazzah and S. Marcos, "Cramer-Rao bounds for antenna array design," *IEEE Trans. Signal Process.*, vol. 54, no. 1, pp. 336–345, Jan. 2006.
- [49] Z. Cheng, B. L. S. Shi, Z. He, and J. Li, "Co-design for overlaid MIMO radar and downlink MISO communication systems via Cramer-Rao bound minimization," *IEEE Trans. Signal Process.*, vol. 67, no. 24, pp. 6227–6240, Dec. 2019.
- [50] M. Wang and A. Nehorai, "Coarrays, MUSIC, and the Cramer Rao bound," *IEEE Trans. Signal Process.*, vol. 65, no. 4, pp. 933–946, Feb. 2017.
- [51] L. Zelnik-Manor, K. Rosenblum, and Y. Eldar, "Sensing matrix optimization for block-sparse decoding," *IEEE Trans. Signal Process.*, vol. 59, no. 9, pp. 4300–4312, Sept. 2011.
- [52] G. Li, Z. Zhu, D. Yang, L. Chang, and H. Bai, "On projection matrix optimization for compressive sensing systems," *IEEE Trans. Signal Process.*, vol. 61, no. 11, pp. 2887–2898, Jun. 2013.



**Chao Liu** (Member, IEEE) received the B.S. degree in electronic science and technology from Nanjing University of Information Science and Technology, Nanjing, China, in 2010 and the Ph.D. degree in information and communication engineering from Nanjing University of Science and Technology, Nanjing, China, in 2018.

In 2020, he joined the Pervasive Communication Research Center, Purple Mountain Laboratories, Nanjing 211111, China and is currently a research engineer. His research interests include array signal processing, compressive sensing, radio propagation measurement, and channel modeling.



**Bensheng Yang** (Member, IEEE) received the B.S. degree from Northeastern University, Qinhuangdao, China, in 2013, the M.S. degree from Xidian University, Xi'an, China, in 2016, the Ph.D. degree from Southeast University, Nanjing, China in 2021, all in Electrical Engineering.

From 2016 to 2017, he was an Engineer with Huawei Technologies Co., Ltd., Nanjing, China. Since 2021, he has been with Huawei Software Technologies Co., Ltd., Nanjing, China. His current research interests include electromagnetic vector antenna design, radio propagation measurements, and integrated communications and sensing technologies in Wireless Local Access Networks.



**Peize Zhang** (Member, IEEE) received the B.S. degree from Beijing University of Posts and Telecommunications, Beijing, China, in 2015, the M.S. degree from China Academy of Telecommunications Technology, Beijing, China, in 2018, and the Ph.D. degree from Southeast University, Nanjing, China in 2022, all in Electrical Engineering.

From 2016 to 2018, he was also a research assistant with the China Academy of Information and Communications Technology, Beijing, China. In 2021, he was a visiting Ph.D. student at the Université catholique de Louvain, Louvain-la-Neuve, Belgium. His current research interests focus on propagation measurement, deployment, and performance analysis of millimeter-wave wireless communication systems.



**Haiming Wang** (Member, IEEE) was born in 1975. He received the B.S., M.S., and Ph.D. degrees in Electrical Engineering from Southeast University, Nanjing, China, in 1999, 2002, and 2009, respectively.

He joined the School of Information Science and Engineering, Southeast University, Nanjing, China, in 2002, and is currently a distinguished professor. He is also a part-time professor with the Purple Mountain Laboratories, Nanjing, China. He has authored and co-authored over 50 technical publications in IEEE TRANSACTIONS ON ANTENNAS AND PROPAGATION, IEEE TRANSACTIONS ON COMMUNICATIONS, and other peer-reviewed academic journals. Prof. Wang has authored and co-authored over more than 80 patents and 56 patents have been granted. He was twice awarded for contributing to the development of IEEE 802.11 by the IEEE Standards Association in 2018 and 2021.

His current research interests include AI-powered antenna and radio-frequency technologies, AI-powered channel measurement and modeling technologies, and integrated communications and sensing technologies.



**Cheng-Xiang Wang** (Fellow, IEEE) received the B.Sc. and M.Eng. degrees in communication and information systems from Shandong University, Jinan, China, in 1997 and 2000, respectively, and the Ph.D. degree in wireless communications from Aalborg University, Aalborg, Denmark, in 2004.

He was a Research Assistant with the Hamburg University of Technology, Hamburg, Germany, from 2000 to 2001, a Visiting Researcher with Siemens AG Mobile Phones, Munich, Germany, in 2004, and a Research Fellow with the University of Agder, Grimstad, Norway, from 2001 to 2005. He has been with Heriot-Watt University, Edinburgh, U.K., since 2005, where he was promoted to a Professor in 2011. In 2018, he joined Southeast University, Nanjing, China, as a Professor. He is also a part-time Professor with Purple Mountain Laboratories, Nanjing. He has authored 4 books, 3 book chapters, and more than 460 papers in refereed journals and conference proceedings, including 25 highly cited papers. He has also delivered 23 invited keynote speeches/talks and 10 tutorials in international conferences. His current research interests include wireless channel measurements and modeling, 6G wireless communication networks, and electromagnetic information theory.

Prof. Wang is a Member of the Academia Europaea (The Academy of Europe), a Fellow of the Royal Society of Edinburgh, IEEE, IET, and China Institute of Communications (CIC), an IEEE Communications Society Distinguished Lecturer in 2019 and 2020, a Highly-Cited Researcher recognized by Clarivate Analytics in 2017-2020, and one of the most cited Chinese Researchers recognized by Elsevier in 2021. He is currently an Executive Editorial Committee Member of the IEEE TRANSACTIONS ON WIRELESS COMMUNICATIONS. He has served as an Editor for over ten international journals, including the IEEE TRANSACTIONS ON WIRELESS COMMUNICATIONS, from 2007 to 2009, the IEEE TRANSACTIONS ON VEHICULAR TECHNOLOGY, from 2011 to 2017, and the IEEE TRANSACTIONS ON COMMUNICATIONS, from 2015 to 2017. He was a Guest Editor of the IEEE JOURNAL ON SELECTED AREAS IN COMMUNICATIONS, Special Issue on Vehicular Communications and Networks (Lead Guest Editor), Special Issue on Spectrum and Energy Efficient Design of Wireless Communication Networks, and Special Issue on Airborne Communication Networks. He was also a Guest Editor for the IEEE TRANSACTIONS ON BIG DATA, Special Issue on Wireless Big Data, and is a Guest Editor for

the IEEE TRANSACTIONS ON COGNITIVE COMMUNICATIONS AND NETWORKING, Special Issue on Intelligent Resource Management for 5G and Beyond. He has served as a TPC Member, a TPC Chair, and a General Chair for more than 80 international conferences. He received 14 Best Paper Awards from IEEE GLOBECOM 2010, IEEE ICCT 2011, ITST 2012, IEEE VTC 2013Spring, IWCMC 2015, IWCMC 2016, IEEE/CIC ICC 2016, WPMC 2016, WOCC 2019, IWCMC 2020, WCSP 2020, CSPPS2021, and WCSP 2021. Also, he received the 2020-2022 "AI 2000 Most Influential Scholar Award Honourable Mention" in recognition of his outstanding and vibrant contributions in the field of Internet of Things.



**Xiaohu You** (Fellow, IEEE) received his Master and Ph.D. Degrees from Southeast University, Nanjing, China, in Electrical Engineering in 1985 and 1988, respectively. Since 1990, he has been working with National Mobile Communications Research Laboratory at Southeast University, where he is currently professor and director of the Lab. He has contributed over 100 IEEE journal papers and 3 books in the areas of adaptive signal processing, neural network and wireless communications. From 1999 to 2002, he was the Principal Expert of the C3G Project.

From 2001-2006, he was the Principal Expert of the China National 863 Beyond 3G FuTURE Project. From 2013 to 2019, he was the Principal Investigator of China National 863 5G Project. His current research interests include wireless networks, advanced signal processing and its applications.

Dr. You was selected as IEEE Fellow in 2011. He was a recipient of the National First Class Invention Prize in 2011. He served as the General Chair for the IEEE Wireless Communications and Networking Conference (WCNC) 2013, the IEEE Vehicular Technology Conference (VTC) 2016 Spring, and the IEEE International Conference on Communications (ICC) 2019. He is currently the Secretary General of the FuTURE Forum, and the Vice Chair of the China IMT-2020 (5G) Promotion Group and the China National Mega Project on New Generation Mobile Network. Dr. You won the IET Achievement Medal in 2021.